Organic Electronics 11 (2010) 1288–1295

Contents lists available at ScienceDirect

Organic Electronics

journal homepage: www.elsevier.com/locate/orgel

4,4′,4″-Tris(4-naphthalen-1-yl-phenyl)amine as a multifunctional material for organic light-emitting diodes, organic solar cells, and organic thin-film transistors

Jongchul Kwon [a], Myoung Ki Kim [a], Jung-Pyo Hong [a], Woochul Lee [a], Seunguk Noh [b], Changhee Lee [b], Seonghoon Lee [a], Jong-In Hong [a,*]

[a] Department of Chemistry, College of Natural Sciences, Seoul National University, Seoul 151-747, Republic of Korea
[b] School of Electrical Engineering and Computer Science, Inter-university Semiconductor Research Center, Seoul National University, Seoul 151-742, Republic of Korea

ARTICLE INFO

Article history:
Received 15 January 2010
Received in revised form 1 April 2010
Accepted 1 April 2010
Available online 9 April 2010

Keywords:
Multifunctional organic semiconductor
Organic solar cells
Organic light-emitting diodes
Organic thin-film transistor

ABSTRACT

We have developed the first multifunctional organic material, 4,4′,4″-tris(4-naphthalen-1-yl-phenyl)amine (**1-TNPA**), which can be used as a deep blue emitting and hole-transporting material in organic light-emitting diodes (OLEDs), as a donor material in organic solar cells (OSCs), and as an active material in organic thin-film transistors (OTFTs). In particular, in the case of **1-TNPA**-based OLEDs, efficient emission characteristics, the emission of deep-blue light similar to the National Television Standard Committee (NTSC) standard blue, and more efficient hole transport than that in the case of NPD-based OLEDs were observed. **1-TNPA** can be also used as a donor in OSCs and as an organic semiconductor in OTFTs.

© 2010 Elsevier B.V. All rights reserved.

1. Introduction

Arylamine-based organic semiconductors [1] have been widely investigated for their optoelectronic applications; owing to their light-absorbing, light-emitting, hole-transporting, and charge carrying transport properties, their use in organic solar cells (OSCs) [2,3], light-emitting [4] and hole-transporting [5,6] materials in organic light-emitting diodes (OLEDs), and organic thin-film transistors (OTFTs) [7], respectively, has been studied. In particular, among the arylamine derivatives, triphenylamine (TPA) derivatives have been used as light-emitting OSC materials [8], or as both emitting and hole-transporting materials in OLEDs [9].

When one considers the manufacturing process of organic electronic devices, one important issue would be the low cost and simple device fabrication. For example, multifunctional organic materials can be utilized in the area of radio-frequency identification tags (RFIDs) manufactured using an all-in-line printing process [10]. The RFIDs manufacturing technology consists of rectifiers, antennas, powering devices, transistors, and encapsulation layers, all integrated into a plastic foil or paper. Since a series of more than ten patterning, material deposition and post-processing steps are required for the fabrication of one kind of device, more than 50 discrete manufacturing steps would be included in the fabrication of RFIDs devices. Thus, an enormous cost cannot be avoided for this RFIDs technology. The difficulties can be overcome by introducing multifunctional materials that can be used in different devices in parallel. Further, this would result in much simpler electronic systems. In general, multifunctional materials [10] with optoelectronic applications such as OLEDs, OSCs, and OTFTs must have light-emitting, light-absorbing, and hole-transporting properties. Since the operational mechanisms of OLEDs, OSCs, and OTFTs are different, it is generally hard to extensively use the same organic

* Corresponding author. Tel.: +82 2 880 6682; fax: +82 2 889 1568.
E-mail address: jihong@snu.ac.kr (J.-I. Hong).

1566-1199/$ - see front matter © 2010 Elsevier B.V. All rights reserved.
doi:10.1016/j.orgel.2010.04.005

materials as active layers in several different devices. Therefore, only a few bi-functional or tri-functional organic materials have been developed thus far [11,2b,12]. To the best of our knowledge, triarylamine derivatives have not been used as multifunctional materials such as light-emitting and hole-transporting materials in OLEDs, donor materials in OSCs, and organic semiconductors in OTFTs.

Here, we report the first example of a multifunctional material that can be used as a deep blue emitting and hole-transporting material in OLEDs, a donor material in OSCs, and an active material in OTFTs. In particular, an OLED device derived from 4,4′,4″-tris(4-naphthalen-1-yl-phenyl)amine (**1-TNPA**) emitted blue light similar to the National Television Standard Committee (NTSC) standard blue and exhibited good electroluminescence (EL) efficiency compared to known blue fluorescent dopants [13–15]. Furthermore, in the case of **1-TNPA**, more efficient hole transport, compared to 4,4′-bis[*N*-(naphthyl-*N*-phenyl amino)]biphenyl (NPD), was observed [5,6,16]. Further, **1-TNPA** can be used as a donor in OSCs and as an organic semiconductor in OTFTs.

2. Experimental section

2.1. Materials and instruments

Organic compounds such as C_{60}, CuPc, NPD, BCP, Alq_3, and ADN were purchased from Aldrich, Lumtree, and Gracel Display. Absorption (UV) spectra were recorded on a Beckman DU 650 spectrophotometer. PL spectra were recorded on a Jasco FP-7500 spectrophotometer. CV spectra were obtained using a CH Instruments 660 electrochemical analyzer. AFM experiments were performed using an Asylum MFP-3D instrument in AC mode and XRD analyses were carried out using a Rigaku (λ = 1.5418 Å; 298 K) X-ray instrument. Decomposition temperatures (T_d) and glass transition temperatures (T_g) were obtained using Q-5000-IR thermal gravimetric analysis (TGA) and DSC-Q-1000 differential scanning calorimetry (DSC), respectively. These TGA and DSC analyses were performed at 5 °C min^{-1} under a N_2 atmosphere.

2.2. Synthesis

4,4′,4″-Tris(4-naphthalen-1-yl-phenyl)amine (**1-TNPA**): a mixture of tris(4-bromophenyl)amine (2.00 g, 4.14 mmol), 1-naphthaleneboronic acid (2.50 g, 14.5 mmol), potassium carbonate (2 M, 20 mL), and tetrakis(triphenylphosphine) palladium (238 mg, 0.206 mmol) in THF/H_2O was heated at 80 °C for 24 h. After cooling to room temperature, all the volatiles were evaporated in vacuum and the reaction mixture was extracted with dichloromethane. The organic phase was washed with H_2O and dried over $MgSO_4$. The solvent was evaporated to give the product, which was purified by silica gel column chromatography using a mixture of ethyl acetate and hexane as the eluent (1:20) and then recrystallized from dichloromethane and hexane to give a solid product (yield: 680 mg, 34%). ^{1}H NMR (300 MHz, $CDCl_3$): δ (ppm) 8.17 (d, 9 Hz, 3H), 8.01 (d, 6 Hz, 3H), 7.94 (d, 18 Hz, 3H), 7.61 (d, 9 Hz, 6H), 7.58 (d, 6 Hz, 6H), 7.54 (d, 6 Hz, 6H), 7.51 (d, 12 Hz, 6H). ^{13}C NMR (125 MHz, $CDCl_3$): δ (ppm) 147.0, 140.0, 135.4, 134.1, 131.8, 131.2, 128.5, 127.6, 127.1, 126.2, 126.1, 125.9, 125.6, 124.2. Mass: Calcd. for $C_{48}H_{33}N$ $[M]^+$ 623.2613, HR-Mass: 623.2613.

2.3. Cyclic voltammetry

The electrochemical properties of **1-TNPA** were studied using cyclic voltammetry (CV) in CH_2Cl_2 solutions (1.00 mM) with 0.1 M tetra-*n*-butylammoniumhexafluorophosphate ($TBAPF_6$) as the supporting electrolyte. A glassy carbon electrode was employed as the working electrode and referenced to an Ag reference electrode. All potential values were calibrated against the ferrocene/ferrocenium (Fc/Fc^+) redox couple.

2.4. Blue OLED device fabrication

A 10-nm-thick layer of copper phthalocyanine (CuPc) was used as a hole injection layer (HIL), and a 60-nm-thick layer of NPD was used as a hole-transporting layer (HTL). A 50-nm-thick emitting layer (EML) was prepared by using 9,10-di(2-naphthyl)anthracene (ADN) as a host and 5–12 wt% **1-TNPA** as a fluorescent blue dopant. The fluorescent dopant concentration of **1-TNPA** was varied from 5 wt% to 12 wt%. Next, a 20-nm-thick tris(8-hydroxyquinolinato)aluminum (Alq_3) layer, which served as an electron transporting layer (ETL), was evaporated. Then, a LiF layer, which served as an electron injection layer (EIL), was also evaporated. Finally, a 100-nm-thick Al layer was deposited onto the LiF layer (Fig. S1). The emission properties were determined using a PR-650 spectrascan spectracolorimeter as a source meter.

2.5. Green OLED device fabrication

A 70-nm-thick NPD layer and a 70-nm-thick **1-TNPA** layer were used as a reference HTL and as a new HTL, respectively. Next, a 60-nm-thick Alq_3 layer was evaporated as an electron transporting layer and a green emitting layer. Then, LiF as an electron injection layer was also evaporated. Finally, a 100-nm-thick Al layer was deposited onto the LiF layer (Fig. S2).

2.6. OSC device fabrication

A 30-nm-thick poly(3,4-ethylenedioxythiophene) poly(styrenesulfonate) (PEDOT:PSS) layer was used as a hole injection layer (HIL). Various **1-TNPA** layers with thicknesses from 10 nm to 20 nm were prepared by evaporation. Then, a 40-nm-thick fullerene (C_{60}) layer, which served as an acceptor, was also evaporated. Next, a 5-nm-thick 2,9-dimethyl-4,7-diphenyl-1,10-phenanthroline (BCP) layer, which served as an exciton blocking layer (EBL), was evaporated. Finally, a 100-nm-thick Al layer was evaporated onto the BCP layer (Fig. S3). The current–voltage measurements for the devices were performed on a Keithley 237 instrument. The device performances were characterized under uniform illumination (AM 1.5G illumination intensity of 100 mW cm^{-2}) using a solar simulator

(Newport, 91160A). The light intensity at each wavelength was calibrated using the standard Si solar cell as a reference.

2.7. OTFT device fabrication

We used a heavily doped Si wafer as a gate electrode and a SiO_2 or an octadecyltrichlorosilane (OTS)-pretreated SiO_2 layer (thickness: ca. 300 nm) as the gate dielectric. The **1-TNPA** films (thickness: ca. 500 Å) were grown by vacuum sublimation at rates of 0.4–0.8 Å s^{-1} under a working pressure of 2.0–2.5 $\times$ 10^{-6} torr using an apparatus devised in our laboratory. Au source/drain electrodes with a channel length (L) of 50 μm and a channel width (W) of 1000 μm were evaporated on top of the films through a shadow mask. The electrical characterization of the transistors was performed in air at room temperature using a Keithley 4200-SCS semiconductor analyzer. The field-effect mobility (μ) was calculated in the saturation region (V_{DS} = −100 V) from a plot of the square-root of drain current *vs.* V_{GS} by using the following equation: $I_{DS} = (WC_i\mu(V_{GS} - V_T)^2)/2L$, where I_{DS} is the source–drain saturation current; C_i (1.1 $\times$ 10^{-8} F) is the capacitance of the SiO_2 insulator; W/L is the ratio of the channel width to the channel length; and V_{GS} and V_T are the gate–source and threshold voltages, respectively.

3. Results and discussion

3.1. Synthesis and photophysical properties

Scheme 1 shows the synthesis of **1-TNPA** examined in this study. A mixture of tris(4-bromophenyl)amine, 1-naphthaleneboronic acid, potassium carbonate, and tetrakis(triphenylphosphine)palladium was refluxed in a N_2 atmosphere in tetrahydrofuran/water solution to afford **1-TNPA** in 34% yield. The photophysical properties of **1-TNPA** are shown in Fig. 1. The absorption spectrum of **1-TNPA** in dichloromethane shows intense bands at 279 nm and 340 nm. The photoluminescence (PL) spectrum of **1-TNPA** in dichloromethane shows a deep blue emission at 436 nm. The full width at half maximum (FWHM) of **1-TNPA** in dichloromethane solution is 63 nm. The PL quantum yield of **1-TNPA** in ethanol solution was estimated to be 0.22 using anthracene as a standard [17].

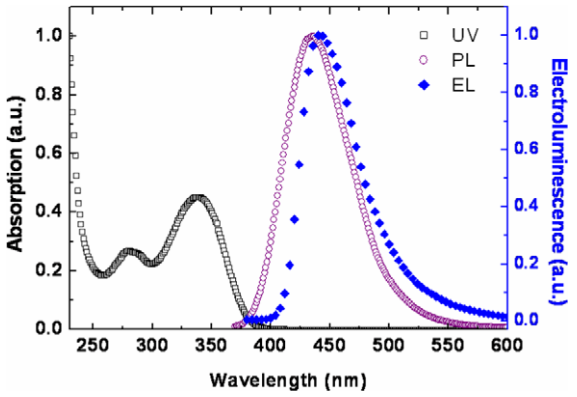

Fig. 1. UV and PL spectra of **1-TNPA** (0.02 mM) in dichloromethane and EL spectra of 3% **1-TNPA**-doped device.

3.2. Thermal and electrochemical properties

The thermal stability of **1-TNPA** was investigated by TGA and DSC. **1-TNPA** shows a thermal stability of T_d = 470 °C, as revealed by the TGA thermogram (Fig. S10), which suggests that **1-TNPA** is stable during the vacuum thermal sublimation process used in organic semiconductor fabrication. When the sample of **1-TNPA** was heated, an endothermic peak was observed at around 176 °C. However, no crystallization and glass transition were observed in the DSC analysis. When the heated sample of **1-TNPA** was cooled to room temperature, it formed an amorphous glass. When the glass sample of **1-TNPA** was heated again, glass transition took place at around 109 °C (Fig. S11). DSC experiments revealed that **1-TNPA** has the property of an amorphous glass with a glass transition temperature (T_g) of 109 °C and therefore no crystallinity.

Fig. 2 shows the cyclic voltammogram of **1-TNPA** in dichloromethane. **1-TNPA** undergoes a reversible oxidation process associated with stable cation radical generation. The half oxidation potentials ($E_{1/2,ox}$) of **1-TNPA**, NPD, and ferrocene were observed to be 0.76 V, 0.59 V, and 0.31 V, respectively (Figs. 2 and S12). Therefore, the highest occupied molecular orbital (HOMO) energy values of **1-TNPA** and NPD were calculated to be $E_{HOMO} = -[(1.4 \pm 0.1) \times (0.45) - (4.6 \pm 0.08)\,eV] = -5.23$ and $E_{HOMO} = -[(1.4 \pm 0.1) \times (0.28) - (4.6 \pm 0.08)\,eV] = -5.00$ eV, respectively [18]. However, the half reduction potential was not determined from CV measurements. The lowest

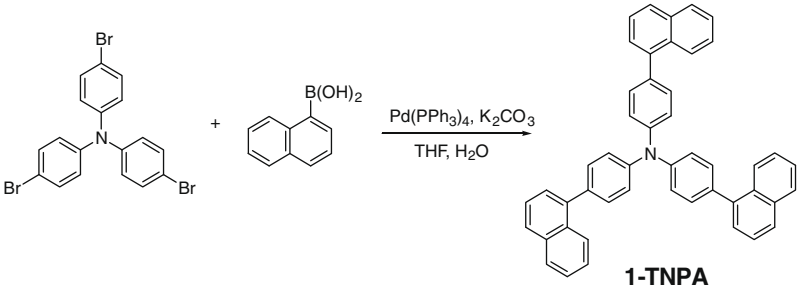

Scheme 1. Synthesis of **1-TNPA**.

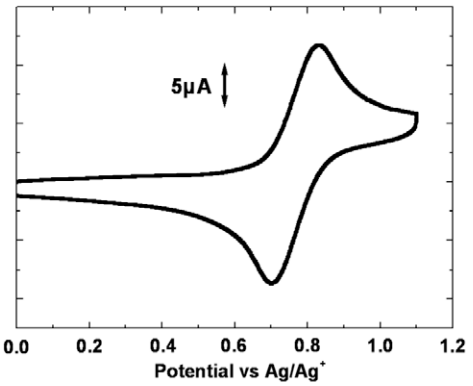

Fig. 2. Cyclic voltammogram of 1.00 mM **1-TNPA** in dichloromethane.

unoccupied molecular orbital (LUMO) energy value of **1-TNPA** (−3.27 eV) was determined from the cross-sectional wavelength between the absorption and emission spectra.

3.3. Blue emitting material in OLEDs

To investigate the versatility of **1-TNPA** as an organic semiconductor, we fabricated four types of organic electronic devices using **1-TNPA**: blue and green emitting OLEDs, an OSC, and an OTFT. To investigate the blue emitting property of **1-TNPA**, we fabricated blue fluorescent OLEDs with the configuration of ITO/CuPc (10 nm)/NPD (60 nm)/emitting layer (50 nm)/Alq_3 (20 nm)/LiF (1 nm)/Al (100 nm). Emitting layers were prepared by co-evaporating ADN as a host and *x* wt% **1-TNPA** as a fluorescent dopant.

Fig. S5 shows the PL in dichloromethane and EL spectra for different doping ratios of **1-TNPA**. All the EL spectra show a deep blue emission. These results indicate that hole–electron recombination takes place at the **1-TNPA** layer. The FWHM of the EL spectrum for 3% **1-TNPA** doping is 61 nm. Since the FWHMs of PL and EL spectra are similar, we attribute the blue EL to the intrinsic emission of **1-TNPA** with no emission interference from Alq_3 [13b]. In particular, the 3% **1-TNPA**-doped EL device showed a pure blue emission with Commission Internationale de l'Eclairage (CIE) coordinates of (0.15, 0.12) at a current density of 6.3 mA cm^{-2}, which is similar to the NTSC standard blue CIE coordinates (0.15, 0.09). Similarly, for a device with 5−8% **1-TNPA** doping, the EL spectra also show the deep blue emission. Since the EL spectra of **1-TNPA** devices with different doping levels have similar patterns, it is suggested that the EL spectra should be attributed to emission from an excited state of **1-TNPA** in the emitting layer. On the other hand, the EL device showed blue emission centered at around 460 nm (Fig. S5) for 10−12% **1-TNPA** doping. As the doping ratio of **1-TNPA** was increased from 3% to 12%, the λ_{max} of the EL spectra was slightly red-shifted because of the aggregation of **1-TNPA** dopant molecules in the emitting layer. This could be due to the molecular structure of **1-TNPA**, which cannot prevent the aggregation in the emitting layer.

Fig. 3 shows plots of the current density (mA cm^{-2}) *vs.* current efficiency (cd A^{-1}) and current density (mA cm^{-2}) *vs.* external quantum efficiency (%) characteristics of ITO/CuPc (10 nm)/NPD (60 nm)/EML (ADN + **1-TNPA** = 50 nm)/Alq_3 (20 nm)/LiF (1 nm)/Al (100 nm) devices. The EL performances depend on the doping ratio of **1-TNPA** in the emitting layer. The optimized 3% **1-TNPA**-doped device had a maximum current efficiency of 3.1 cd A^{-1} and an external quantum efficiency of 3.0% at a current density of 3.4 mA cm^{-2}. At this doping ratio, maximum EL efficiency and a blue emission similar to NTSC blue were observed. We attribute the improved EL performance to the greater charge balance and better exciton confinement within the emission layer. A comparison of the EL device, involving the use of **1-TNPA** as a fluorescent dopant, with the known NTSC standard deep blue fluorescent dopant materials reveals that the current efficiency of 3.1 cd A^{-1} and the external quantum efficiency of 3.0% are generally satisfactory [13–15]. The 8% **1-TNPA**-doped EL device had a slightly reduced current efficiency of 2.5 cd A^{-1} and an external quantum efficiency of 2.3% at a current density of 4.3 mA cm^{-2}. The 12% **1-TNPA**-doped EL device had a current efficiency of 2.1 cd A^{-1} and an external quantum efficiency of 1.7% at 4.7 mA cm^{-2}. When the doping ratio of **1-TNPA** changed from 3% to 12%, the current efficiency and external quantum efficiency slightly decreased from 3.1 cd A^{-1} to 2.1 cd A^{-1} and from 3% to 1.7%, respectively. The relatively reduced EL efficiency can be attributed to a

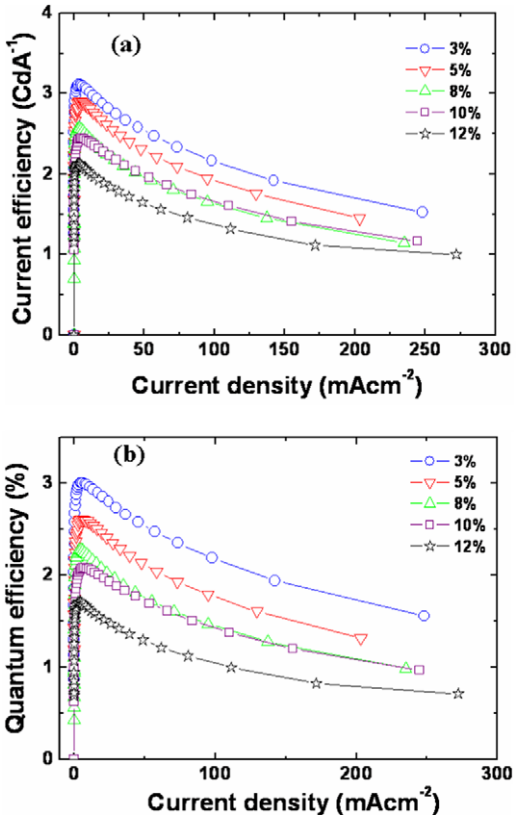

Fig. 3. A blue emitting EL device with configuration ITO/CuPc (10 nm)/NPD (60 nm)/EML (ADN:**1-TNPA** = 50 nm)/Alq_3 (20 nm)/LiF (1 nm)/Al (100 nm). (a) Current density (mA cm^{-2}) *vs.* current efficiency (cd A^{-1}) characteristics and (b) current density (mA cm^{-2}) *vs.* external quantum efficiency (%) characteristics.

Table 1
Blue emitting OLED data.

	η_p (lm W^{-1})[a]	η_c (cd A^{-1})[b]	η_{ext} (%)[c]	η_L (cd m^{-2})[d]	EL (λ_{nm})	CIE
3%	1.0	3.1	3.0	3784	440	(0.15, 0.12)
5%	0.9	2.7	2.5	2945	456	(0.16, 0.13)
8%	0.8	2.5	2.3	2694	456	(0.16, 0.14)
10%	0.7	2.4	2.0	2849	460	(0.16, 0.15)
12%	0.6	2.1	1.7	2717	460	(0.16, 0.17)

Device structure: ITO/CuPc (10 nm)/NPD (60 nm)/EML (50 nm)/Alq_3 (20 nm)/LiF (1 nm)/Al (100 nm).
[a] Power efficiency at 100 cd m^{-2}.
[b] Current efficiency at 100 cd m^{-2}.
[c] External quantum efficiency at 100 cd m^{-2}.
[d] Maximum luminance.

less balanced hole and electron recombination at the emitting layer caused by the aggregation of **1-TNPA** dopant molecules. The entire EL device data are summarized in Table 1; the data indicate that **1-TNPA** can be used as an efficient deep blue emitting material.

3.4. Hole-transporting material in green emitting OLEDs

Recently, NPD has been widely used as a standard hole-transporting material in OLEDs [5,6,16]. In this study, in order to compare the hole-transporting properties of **1-TNPA** with those of NPD, we fabricated two types of fluorescent OLEDs with the configuration of ITO/**1-TNPA** or NPD (70 nm)/Alq_3 (60 nm)/LiF (1 nm)/Al (100 nm). Figs. 4(a) and S8 show the EL spectra and CIE coordinates of the NPD- and **1-TNPA**-based OLED devices. The EL spectra of both the **1-TNPA**- and NPD-based devices showed identical green emissions centered at 528 nm, and the CIE coordinates of both **1-TNPA**- and NPD-based devices were almost equal. The similar EL spectra and CIE coordinates of NPD- and **1-TNPA**-based devices suggest that the EL spectra and CIE coordinates should be attributed to an emission from an excited state of Alq_3 in the emitting layer. This indicates that **1-TNPA** can also be used as a hole-transporting material in green emitting OLEDs.

Fig. 4(b) shows that the maximum current efficiency of the **1-TNPA**-based device is 4.4 cd A^{-1}, which is 45% higher than that of the NPD-based reference device (3.0 cd A^{-1} at 25 mA cm^{-2}). Fig. S7(e) shows that the maximum power efficiency of the **1-TNPA**-based device is 2.0 lm W^{-1}, which is 33% higher than that of the NPD-based reference device (1.5 lm W^{-1} at 25 mA cm^{-2}, Table 2). The enhancement of both current efficiency and power efficiency when using **1-TNPA** as the hole-transporting material can be attributed to a more balanced recombination of holes and electrons at the emitting layer because of the formation of a hole blocking barrier which results from the low HOMO energy level of **1-TNPA**. This finding is supported by the current density *vs.* voltage data (Fig. S7(g)); at all voltages, the **1-TNPA**-based device shows a lower current density than the NPD-based reference device [5a]. Also, the turn-on voltage of the **1-TNPA**-based device (2.6 V) was slightly lower than that of the NPD-based reference device (2.8 V) because of a more balanced hole and electron recombination in the emitting layer. The **1-TNPA** device needs a higher voltage than the

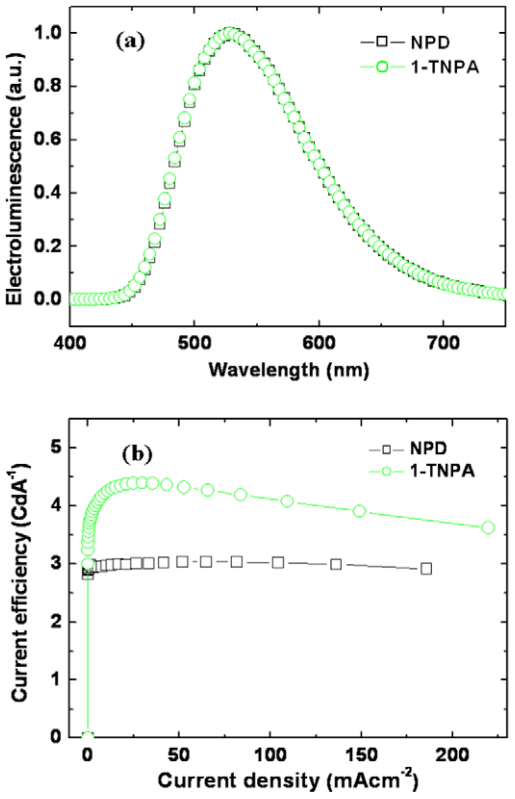

Fig. 4. A green emitting EL device with configuration ITO/NPD or **1-TNPA** (70 nm)/Alq_3 (60 nm)/LiF (1 nm)/Al (100 nm). (a) EL spectra and (b) current density (mA cm^{-2}) *vs.* current efficiency (cd A^{-1}) characteristics.

NPD-based reference device for these two devices to have the same current density or luminance. It is because the HOMO (−5.23 eV) energy level of **1-TNPA** is lower than that of NPD (−5.00 eV) and results in a higher hole blocking barrier which consequently retards the hole-transporting in the **1-TNPA**-based device. Therefore, **1-TNPA** can be used in green emitting OLEDs as a better hole-transporting material when compared to NPD.

3.5. Donor material in OSCs

To investigate the photovoltaic effect of **1-TNPA**, we fabricated OSCs with the configuration of ITO/PEDOT:PSS (30 nm)/**1-TNPA** (*x* nm)/C_{60} (40 nm)/BCP (5 nm)/Al (100 nm).

Table 2
Green emitting OLED data.

	η_p (lm W^{-1})[c]	η_c (cd A^{-1})[d]	η_{ext} (%)[e]	η_L (cd m^{-2})[f]	EL (λ_{nm})	CIE
NPD[a]	1.5	3.0	1.1	5409	528	(0.34, 0.53)
1-TNPA[b]	2.0	4.4	1.7	7956	528	(0.35, 0.53)

[a] ITO/NPD (70 nm)/Alq_3 (60 nm)/LiF (1 nm)/Al (100 nm).
[b] ITO/**1-TNPA** (70 nm)/Alq_3 (60 nm)/LiF (1 nm)/Al (100 nm).
[c] Power efficiency at 100 cd m^{-2}.
[d] Current efficiency at 100 cd m^{-2}.
[e] External quantum efficiency at 100 cd m^{-2}.
[f] Maximum luminance.

Fig. 5 shows the current–voltage characteristics of **1-TNPA**- and C_{60}-based heterojunction solar cells under AM 1.5 simulated solar illumination (intensity: 100 mW cm^{-2}). All the devices show photovoltaic behavior. In general, increasing the active-layer thickness increases the absorption ability; however, the absorption will be limited by the slow charge transport and separation in the active layer of the heterojunction device. Thus, it is important to optimize the active-layer thickness to improve the power conversion efficiency of the heterojunction devices. The 10-nm **1-TNPA**-based device had a short circuit current (I_{sc}) of 1.02 mA cm^{-2}, an open circuit voltage (V_{oc}) of 0.72 V, and a fill factor (FF) of 28%; from these data, the power conversion efficiency (PCE) was determined to be 0.21%, and this was attributed to the thin **1-TNPA** film. In the case of the thin **1-TNPA** active layer (10 nm), the absorption of the sunlight is reduced. The optimized **1-TNPA**-based device (film thickness: 15 nm) had an increased short circuit current of 1.35 mA cm^{-2} and an open-circuit voltage of 0.87 V; the FF was 38%. From these data, an increased maximum power conversion efficiency of 0.45% was calculated. By contrast, the device with a 20-nm **1-TNPA** active layer had a slightly reduced short circuit current of 1.3 mA cm^{-2}, an open-circuit voltage of 0.70 V, and an FF of 39%; from these data, a slightly reduced power conversion efficiency of 0.36%, which is attributed to the thicker thin film, was calculated. In the case of the thick **1-TNPA** active layer, effective charge transport and separation were affected, and they were limited by the low charge carrier mobility and diffusion length. In this study, the optimal thickness of the **1-TNPA** layer (15 nm) results in a maximum power conversion efficiency of 0.45%. Therefore, the change in the thickness of the **1-TNPA** film in the active layer changed the power conversion efficiency from 0.21% to 0.45%. Overall, the power conversion efficiency of **1-TNPA**-based OSCs was not high compared with other small-molecule-based OSCs because of the short absorption range (250–370 nm) and poor crystalline property of **1-TNPA**. Nevertheless, to the best of our knowledge, there are no reports of organic electronic materials that act as blue emitting materials as well as hole-transporting materials in OLEDs and donor materials in

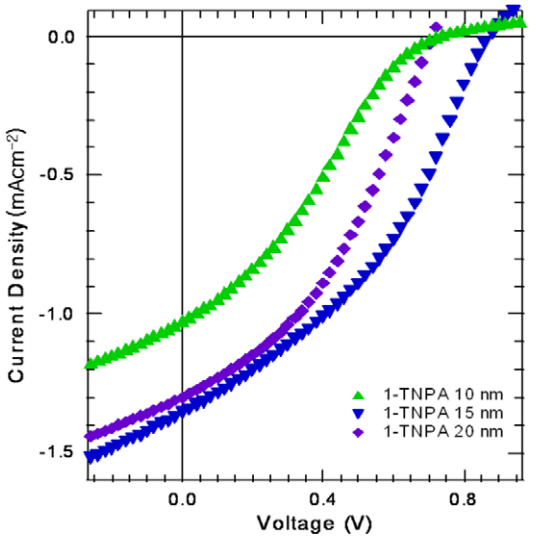

Fig. 5. Current–voltage characteristics of ITO/PEDOT (30 nm)/**1-TNPA** (x nm)/C_{60} (40 nm)/BCP (5 nm)/Al (100 nm) devices under simulated AM 1.5 solar irradiation at 100 mW cm^{-2}.

Table 3
OSC data.

1-TNPA (nm)	V_{oc} (V)[a]	I_{sc} (mA cm^{-2})[b]	FF (%)[c]	PCE (%)[d]
10	0.72	1.02	28	0.21
15	0.87	1.35	38	0.45
20	0.70	1.3	39	0.36

Device structure: ITO/PEDOT (30 nm)/**1-TNPA** (x nm)/C_{60} (40 nm)/BCP (5 nm)/Al (100 nm).
[a] Open circuit voltage.
[b] Short circuit current.
[c] Fill factor.
[d] Power conversion efficiency.

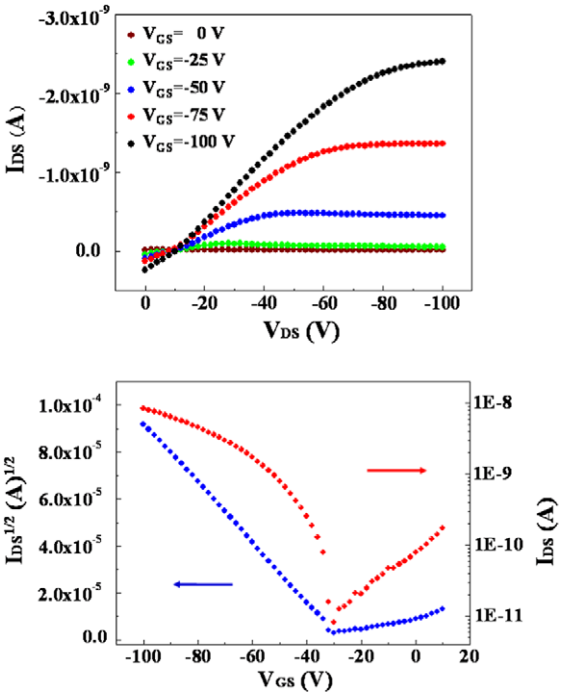

Fig. 6. The output and transfer characteristics of the OTFTs involving the use of **1-TNPA** deposited at T_{sub} = 75 °C on OTS treated SiO_2.

Table 4
Data on OTFTs.

1-TNPA	T_{sub} (°C)	μ (cm^2 V^{-1} s^{-1})[a]	V_{th} (V)[b]	I_{on}/I_{off}[c]
Bare SiO_2	RT	4.2×10^{-6}	−28.3	1.1×10^3
Bare SiO_2	75	3.2×10^{-6}	−27.1	1.3×10^3
OTS/SiO_2	RT	4.7×10^{-6}	−45.4	6.9×10^2
OTS/SiO_2	75	1.5×10^{-5}	−27.6	1.0×10^3

[a] Field-effect mobility.
[b] Threshold voltage.
[c] On/off ratio.

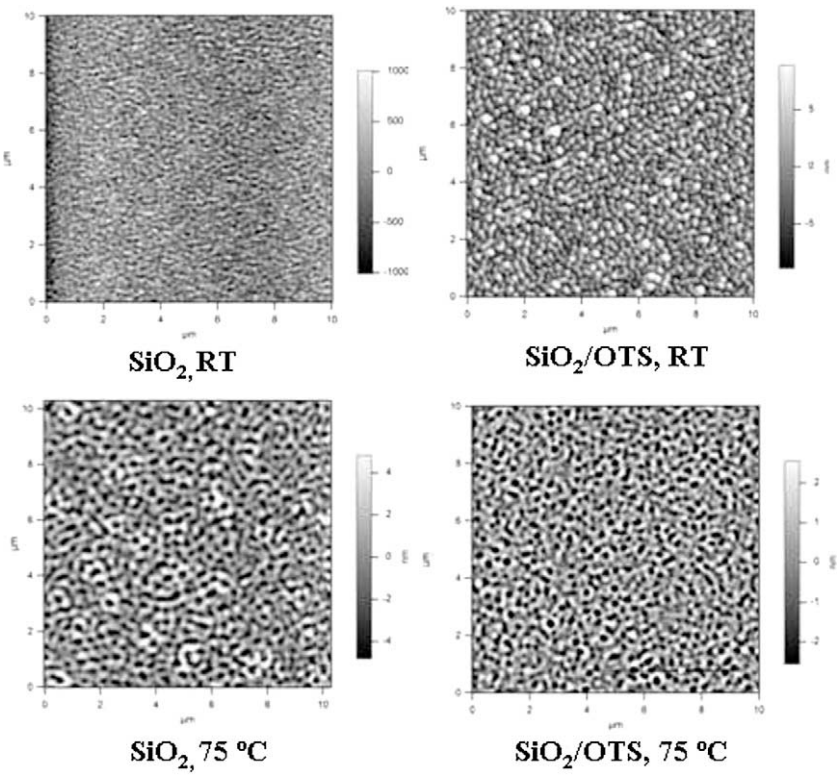

Fig. 7. $10 \times 10\ \mu m^2$ AFM topography images of **1-TNPA** films deposited on SiO_2 (left column) and OTS/SiO_2 (right column) at substrate temperatures equal to RT and 75 °C.

OSCs. The data on the overall performance of **1-TNPA**- and C_{60}-based devices are summarized in Table 3.

3.6. Active material in OTFTs

To investigate the field-effect mobility of **1-TNPA**, we fabricated an OTFT involving the use of **1-TNPA** as an active material with top-contact geometry (Fig. S4). Fig. 6 shows the output and transfer characteristics of top-contact OTFTs involving the use of **1-TNPA** deposited on OTS/SiO_2 at a substrate temperature (T_{sub}) of 75 °C. From the electrical transfer characteristics, we obtained device parameters such as the field-effect mobility, on/off current ratio, and threshold voltage. The **1-TNPA**-based OTFT device showed a field-effect mobility (μ) of $1.5 \times 10^{-5}\ cm^2\ V^{-2}\ s^{-1}$, a threshold voltage ($V_{th}$) of −27.6 V, and an on/off current ratio (I_{on}/I_{off}) of 1.0×10^3 at 75 °C. The moderate field-effect mobilities of the OTFT devices derived from **1-TNPA** and triphenylamine derivatives [7b] can be attributed to the fact that it is difficult to maintain these derivatives perpendicular to the substrate. **1-TNPA**-based OTFTs exhibited similar field-effect mobilities of $1.5 \times 10^{-5}\ cm^2\ V^{-2}\ s^{-1}$, which were moderate compared to those of other triphenylamine derivatives [7b]. The morphological characteristics of **1-TNPA** were investigated by X-ray diffraction (XRD) and atomic force microscope (AFM). The thin-film XRD patterns indicated a poorly ordered structure of **1-TNPA** on the substrate (Fig. S9). Fig. 7 shows AFM images of **1-TNPA** active layers deposited on SiO_2 (left column) and OTS/SiO_2 (right column) at RT and 75 °C. The connectivity of **1-TNPA** grains deposited on a SiO_2 and OTS/SiO_2 substrate at RT and 75 °C is poor, which leads to low field-effect mobility. The data on the **1-TNPA**-based OTFT device for various conditions are summarized in Table 4.

4. Conclusion

We have developed the first multifunctional organic material (**1-TNPA**), which can be used as a deep blue emitting and hole-transporting material in OLEDs, as a donor material in OSCs, and as an active material in OTFTs. In particular, in the case of **1-TNPA**-based devices, efficient, deep blue emission similar to the NTSC standard blue was observed. **1-TNPA** can be used as a hole-transporting material which is more efficient and thermally stable than NPD. **1-TNPA** can be also used as a donor in OSCs and as an organic semiconductor in OTFTs.

Acknowledgements

This work was supported by Basic Science Research Program through the National Research Foundation of Korea (NRF) grant funded from the Ministry of Education, Science and Technology (MEST) of Korea for the Center for Next Generation Dye-sensitized Solar Cells (No. 2010-0001842), the Seoul R&BD Program (10543), the National Research Foundation of Korea Grant funded by the Korean

Government (MEST) (NRF-C1AAA001-2009-0093282). We also acknowledge the BK21 fellowship grants to J.K. and W.L.

Appendix A. Supplementary material

Supplementary data associated with this article can be found, in the online version, at doi:10.1016/j.orgel.2010.04.005.

References

[1] (a) Y. Shirota, J. Mater. Chem. 10 (2000) 1;
(b) Y. Shirota, J. Mater. Chem. 15 (2005) 75.
[2] (a) S. Roquet, A. Cravino, P. Leriche, O. Alévêque, P. Frère, J. Roncali, J. Am. Chem. Soc. 128 (2006) 3459;
(b) A. Cravino, S. Roquet, O. Alévêque, P. Leriche, P. Frère, J. Roncali, Chem. Mater. 18 (2006) 2584;
(c) H. Kageyama, H. Ohishi, M. Tanaka, Y. Ohmori, Y. Shirota, Appl. Phys. Lett. 94 (2009) 063304.
[3] (a) A. Cravino, S. Roquet, P. Leriche, O. Alévêque, P. Frère, J. Roncali, Chem. Commun. (2006) 1416;
(b) C. He, Q. He, X. Yang, G. Wu, C. Yang, F. Bai, Z. Shuai, L. Wang, Y. Li, J. Phys. Chem. C 111 (2007) 8661.
[4] (a) S. Tao, Y. Zhou, C.-S. Lee, S.-T. Lee, D. Huang, X. Zhang, J. Phys. Chem. C 112 (2008) 14603;
(b) J.M. Hancock, A.P. Gifford, Y. Zhu, Y. Lou, S.A. Jenekhe, Chem. Mater. 18 (2006) 4924.
[5] (a) Q.-X. Tong, S.-L. Lai, M.-Y. Chan, K.-H. Lai, J.-X. Tang, H.-L. Kwong, C.-S. Lee, S.-T. Lee, Chem. Mater. 19 (2007) 5851;
(b) J. Li, D. Liu, Y. Li, C.-S. Lee, H.-L. Kwong, S. Lee, Chem. Mater. 17 (2005) 1208;
(c) J. Li, C. Ma, J. Tang, C.-S. Lee, S. Lee, Chem. Mater. 17 (2005) 615.
[6] H. Tsuji, C. Mitsui, L. Ilies, Y. Sato, E. Nakamura, J. Am. Chem. Soc. 129 (2007) 11902.
[7] (a) Y. Song, C. Di, X. Yang, S. Li, W. Xu, Y. Liu, L. Yang, Z. Shuai, D. Zhang, D. Zhu, J. Am. Chem. Soc. 128 (2006) 15940;
(b) M. Sonntag, K. Kreger, D. Hanft, P. Strohriegl, S. Setayesh, D.D. Leeuw, Chem. Mater. 17 (2005) 3031.
[8] A. Cravino, P. Leriche, O. Alévêque, S. Roquet, J. Roncali, Adv. Mater. 18 (2006) 3033.
[9] J.N. Moorthy, P. Venkatakrishnan, D.-F. Huang, T.J. Chow, Chem. Commun. (2008) 2146;
(a) S. Tao, L. Li, J. Yu, Y. Jiang, Y. Zhou, C.-S. Lee, S.-T. Lee, X. Zhang, O. Kwon, Chem. Mater. 21 (2009) 1284.
[10] M. Berggren, D. Nilsson, N.D. Robinson, Nat. Mater. 6 (2007) 4.
[11] (a) A.K. Pandey, J.-M. Nunzi, Adv. Mater. 19 (2007) 3613;
(b) J. Lu, P.F. Xia, P.K. Lo, Y. Tao, M.S. Wong, Chem. Mater. 18 (2006) 6194.
[12] F. Wang, J. Luo, K. Yang, J. Chen, F. Huang, Y. Cao, Macromolecules 38 (2005) 2253.
[13] (a) M.-T. Lee, C.-H. Liao, C.-H. Tsai, C.H. Chen, Adv. Mater. 17 (2005) 2493;
(b) Y.-H. Kim, H.-C. Jeong, S.-H. Kim, K. Yang, S.-K. Kwon, Adv. Funct. Mater. 15 (2005) 1799.
[14] (a) Y.-I. Park, J.-H. Son, J.-S. Kang, S.-K. Kim, J.-H. Lee, J.-W. Park, Chem. Commun. (2008) 2143;
(b) J.N. Moorthy, P. Venkatakrishnan, P. Natarajan, D.-F. Huang, T.J. Chow, J. Am. Chem. Soc. 130 (2008) 17320.
[15] C.-H. Chien, C.-K. Chen, F.-M. Hsu, C.-F. Shu, P.-T. Chou, C.-H. Lai, Adv. Funct. Mater. 19 (2009) 560.
[16] S.A. Van Slyke, C.H. Chen, C.W. Tang, Appl. Phys. Lett. 69 (1996) 2160.
[17] W.R. Dawson, M.W. Windsor, J. Phys. Chem. 72 (1968) 3255.
[18] B.W. D'Andrade, S. Datta, S.R. Forrest, P. Djurovich, E. Polikaropov, M.E. Thompson, Org. Electron. 6 (2005) 11.